Batteries & Supercaps

Research Article
doi.org/10.1002/batt.202300244

Chemistry Europe
European Chemical Societies Publishing

www.batteries-supercaps.org

Special Collection

Facile Preparation of Higher Conductivity Porous Polyimide-based Separators by Phase Inversion and its Overcharge-sensitive Modification for Lithium-ion Batteries

Xiangming Feng,*[a] Mengzhen Wang,[a] Jinyun Zheng,[a] Junmin Ge,[a] Mingrui Yang,[a] and Weihua Chen*[a]

Separator plays multiple roles in the performance and safety of lithium-ion batteries owing to the lower conductivity of the organic electrolyte and the hyperactive electrode materials. However, the commercial polyolefin separator suffers from the poor thermal stability, weak electrolyte-wettability, low porosity as well as the demanding and costly manufacturing. Herein, we demonstrate the facial synthesis of a sponge-like, isotropic, polyimide-based separator by phase inversion, which possessed the higher electrolyte-saturating conductivity (1.74 mS cm^{-1}) and ion transference number (0.81) besides its excellent wettability and thermal stability. Meanwhile, the bearable stress was further promoted by 60% with the 30 wt% epoxy-strengthening tactic and the high porosity (67%) and conductivity (1.47 mS cm^{-1}) still preserved. Additionally, an overcharge-sensitive PI separator was further developed by combining the conductive copolymer of coumarin-triphenylamine by virtue of the eminent processability of PI, which demonstrated the outstanding voltage-restraining capability for $LiFePO_4$-based cell during overcharge. Therefore, polyimide-based separator could be a quite promising candidate due to its facile manufacturing, preferable performance and versatile functionalizing.

Introduction

Lithium-ion batteries (LIBs) have been widely employed in portable electronics,[1] electric vehicles[2] and even power grids[3] as preferable energy storage devices for their outperformance in energy density, longevity and environmental friendliness.[4] However, in terms of the rate behavior, LIBs are far inferior to the conventional aqueous-based batteries owing to the lower conductivity of organic electrolyte (~mS cm^{-1}),[5,6] which require the adoption of ultrathin (<20 μm) and porous separators to minimize the gap between electrodes as much as possible.[7,8]

The microstructure and texture of separator have significant impact on the performance of LIBs.[9–12] On the one hand, abundant micropores are indispensable and also pivotal to conserve electrolyte for the shuttling of lithium ions during charge and discharge. On the other hand, maintaining thermal stability is equally essential, otherwise the thermal shrinkage and melting will engender severe consequence once overheat. In addition, the excellent wettability and electrolyte-saturating capability will be conducive to the rate and cycling performance of LIBs.

Currently, the commercial separators are generally made of polyolefin benefiting from its physical and chemical inertness, which give rise to its demanding and costly manufacturing for its rooted poor fabricability, such as dry and wet processes with uniaxial or biaxial stretching, to create micropores.[13–16] Moreover, the low melting point of polyethylene (PE) at 120 °C and polypropylene (PP) at 160 °C[17] implies that thermal shrinkage could happen at a relatively low temperature. To improve the overall performance and simplify the manufacturing process, numerous studies are being conducted on the materials and preparation methods.[17,18]

Recently, a novel material, polyimide (PI) has drawn attention for its excellent processability,[19] such as mouldability, extrudability, spinnability and stretchability, apart from its outstanding chemical and thermal stability (>200 °C),[20,21] which make it a good candidate as separator. For example, an electrostatic-spun PI separator had been obtained for lithium-ion cells,[22,23] displaying favorable performance. Besides spinnability, its dissolvability in DMSO rather than in water makes it feasible for preparing the porous separator by phase inversion route. Indeed, the PI separator was prepared firstly, and the epoxy-strengthening tactic was also attempted to further improve its strength.[24,25]

In recent years, functionalized separators have been developed as well, one of which is resistant to overcharge by automatically shifting from the insulative and conductive state due to containing conductive polymers, avoiding the irreversible electrochemical oxidation of electrolyte.[26,27] The pertinent investigation showed coumarin-triphenylamine copolymer was applicable for separator of LIBs due to its outstanding electro-

[a] Assoc. Prof. X. Feng, M. Wang, Assoc. Prof. J. Zheng, Dr. J. Ge, Dr. M. Yang, Prof. W. Chen
Green Catalysis Center
College of Chemistry
Zhengzhou University
Zhengzhou, 450001 (P.R. China)
E-mail: fengxm@zzu.edu.cn
chenweih@zzu.edu.cn

Supporting information for this article is available on the WWW under https://doi.org/10.1002/batt.202300244

Special Collection An invited contribution to a Special Collection on Young Scientists in Battery Research

Research Article
doi.org/10.1002/batt.202300244
Chemistry Europe
European Chemical Societies Publishing

chemical activity and proper redox potential (3.75 V vs. Li)[28,29] in $LiFePO_4$-based batteries which have been widely applied in electric vehicles and tentatively in power grids. Therefore, the overcharge-proof PI separator was further developed by integrating the conductive copolymer during the preparation.

Results and Discussion

Preparation, morphology, porosity of PI and epoxy-strengthened separator

Compared with the stretching process, on one hand, the phase inversion almost eliminates the residual stress in separators; on the other hand, the preferable isotropy is achieved, both of which will be conducive to retain the dimensional stability during overheat. The procedure of preparing the PI separator is illustrated in Scheme 1.

By means of phase inversion, the white and flexible PI separators (upper) and the epoxy-strengthened one (lower) were obtained as shown in Figure 1(a), which are similar to the commercial and the electrostatic-spun separators in appearance.[30] However, the microstructure would be distinct conjecturally and a series of samples were prepared with 6.8 wt%–16.7 wt% PI-DMSO solution, defined as 6.8%, 8.4%, 10%, 12%, 14% and 16.7%-PI, respectively, and then examined with SEM, as shown in Figure 1(b_1–b_6).

Different from the electrostatic-spun PI separator[31] and the commercial uniaxially- stretched, dry-processed PP separator, Figure S1, all PI separators exhibit sponge-like microstructure clearly, which are similar to the biaxially stretched PP separator.[17] In addition, the regular contraction of the pore size is also observed in Figure 1(b_1–b_6). More specifically, the 6.8% PI separator exhibits the maximal pore size, more than 1 μm (as shown in Figure 1b_1), 87% porosity, and over 5 times electrolyte uptake rate compared to PP (as shown in Figure 1c). Subsequently, the porosity gradually decreases with the higher PI concentration to 73% porosity of the 14% PI separator, still higher than that of PP which is ~55%.[17] The higher porosity generally means the more channels for lithium ion transportation. The conductivities of the electrolyte-saturated separators are shown in Figure 1(d). As expected, the 6.8% PI separator offers the highest conductivity as much as 2.48 mS cm^{-1} and the 8.4% PI sample offers a little lower conductivity of 1.74 mS cm^{-1}, still far higher than that of the electrolyte-saturated PP, 0.6 mS cm^{-1}.

The higher porosity generally means the lower mechanical strength therefore the lower porosity should be preferred as far as the strength is concerned. However, the separators from the higher concentration PI solution displayed weak flexibility and the resultant higher viscosity of solution also gave rise to the difficulty in controlling the thickness and acquiring the bulk and integral samples. After overall comparison of pore size, conductivity and mechanical strength, the 8.4 wt% PI-DMSO solution was determined for the subsequent investigation. Additionally, in order to further improve the mechanical strength of the PI separator, epoxy-strengthening tactic was tentatively introduced by adding 10 wt%, 20 wt% and 30 wt% epoxy resin into the 8.4 wt% PI-DMSO solution, forming epoxy-strengthened separators labelled as 8.4% PI-10ED, -20ED and -30ED, respectively, to benefit from epoxy's excellent physical-chemical and thermal stability from its three-dimensional cross-linking structure featuring insoluble and non-melting, besides its hydrophilia, easy operation and low cost. The relevant curing reaction was shown in Figure S2. The bearable stress of the epoxy-strengthened separators was tested and plotted in Figure 1(e). Undoubtedly, the minimum strength of 1.55 MPa is obtained for the 6.8% PI sample because of the maximal porosity as well as the doubled strength of 3.1 MPa for the 8.4% PI separator, close to the ultimate tensile strengths of unmodified non-porous high density PE (HDPE) and PP, typically around 3.0 and 3.3 MPa,[17] far higher than 0.81 MPa of Glass Fabric. After epoxy was introduced, the strength is further promoted to 3.6 MPa for 8.4% PI-2ED and to 4.8 MPa for 8.4% PI-3ED sample, maximally 60% improvement. With the introducing of epoxy, the pore size and porosity could be impacted, and the porosity and SEMs are presented in Figure 1(f). As reflected, 10 wt% epoxy has less influence on PI skeleton because of the almost identical microstructure and porosity, but the skeleton is gradually coated with epoxy resin for 20 wt% and 30 wt% samples with the shrunk porosity to 73% and 67%. In the meantime, the cross sections are also exhibited in Figure 1(g and h), showing around 20 μm thickness of 8.4%

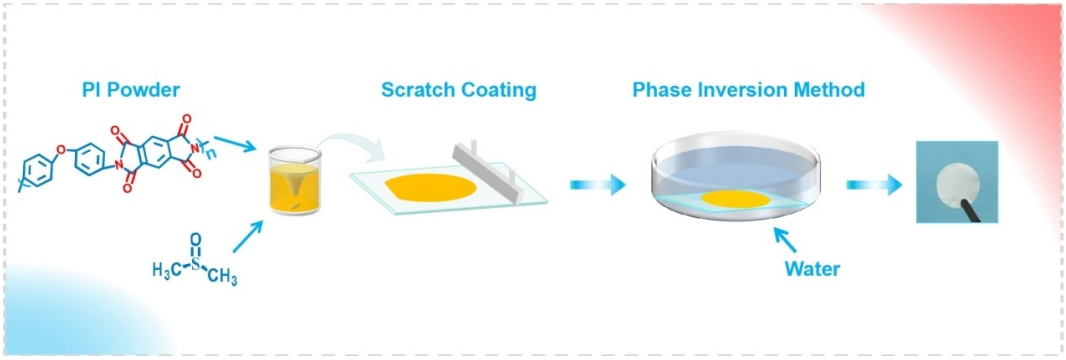

Scheme 1. Schematic illustration of the preparation of PI separator.

Research Article
doi.org/10.1002/batt.202300244
Chemistry Europe
European Chemical Societies Publishing

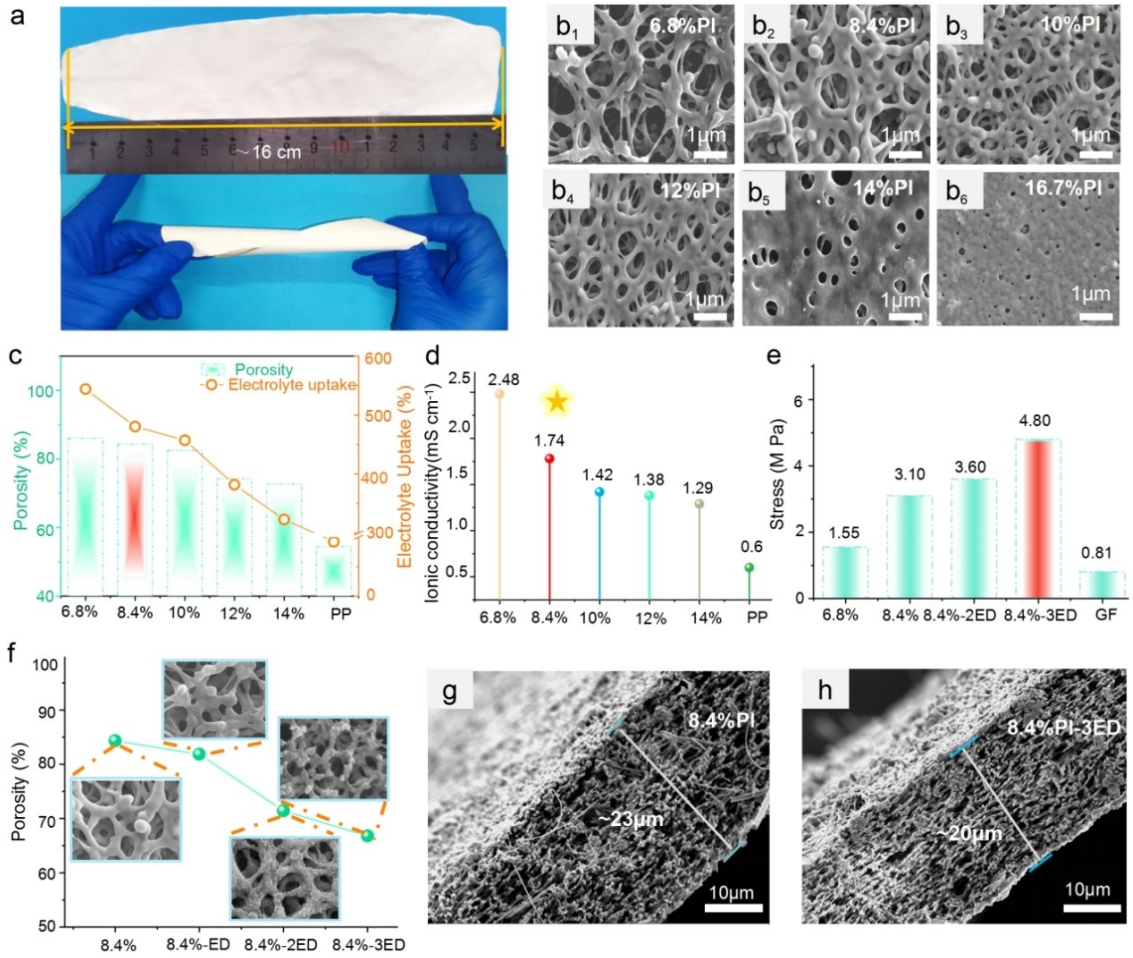

Figure 1. Morphology, porosity and strength of PI and epoxy-strengthened separator, a) photographs of PI (upper) and epoxy-strengthened PI separator (lower); b_1–b_6) SEM of separators from the concentration-diversified PI-DMSO solutions; c) porosity and electrolyte-uptaking rate; d) electrolyte-saturating conductivity; e) strength of PI and epoxy-strengthened separator; f) SEMs and porosity of epoxy-diversified separator; g and h) cross sectional SEMs of PI and 30 wt% epoxy-strengthened separator.

PI and 8.4%-3ED separator, in which the internal spongy microstructure seems to be less altered even by 30 wt% epoxy.

Thermal stability and wetting ability

In respect of thermal stability, thermogravimetric behavior and DSC of 8.4% PI, 8.4% PI-3ED and PP separators were sequentially investigated from 25 °C to 400 °C in Figure 2(a and b).

Although PI and PP demonstrates the favorable thermogravimetric stability to around 360 °C compared with the weight-losing temperature of 8.4% PI-3ED sample, 240 °C, in Figure 2(a), PP starts to melt around 150 °C as indicated with an endothermic peak, 166 °C, in Figure 2(b), which will definitely cause the short-circuit in batteries and then trigger the more severe consequence. Furthermore, the thermal stability of 8.4% PI, 8.4% PI-3ED and PP separators were verified at 25 °C, 135 °C, 180 °C and 200 °C again. Figure 2(c) reflects that PP unevenly shrinks at 135 °C owing to the residual stress and poor isotropy, and thoroughly melts at 180 °C while 8.4% PI and 8.4% PI-3ED separators still remain intact at 200 °C. Additionally, the dissolvability of PI and epoxy-strengthened separator was evaluated by immersion in the ester and ether-based electrolyte for 5 hrs. Figure S3 indicates no dissolving sign is observed.

On the contrary to the electrolyte-repellent polyolefin, PI is strongly hydrophilic due to containing abundant polar groups as reflected in FT-IR, Figure 2(d), such as carbonyl and imine groups, which will be conducive to the electrolyte-saturating and -conserving performance. Therefore, the contact angle with ester-based electrolyte containing Lithium and Sodium salts were respectively measured and presented in Figure 2(e and f), in which 8.4% PI and 8.4% PI-3ED separator display the preferable contact angle of 10°–12°, close to GF, and significantly superior to PP, 34°.

Performance on ion transportation and in Li-based cell

The conductivity of electrolyte-saturated separators is another crucial parameter and was assessed by EIS. Figure 3(a) reveals 1.46 mS cm^{-1} is achieved for 8.4% PI-3ED separator, a little

Research Article
doi.org/10.1002/batt.202300244
Chemistry Europe
European Chemical Societies Publishing

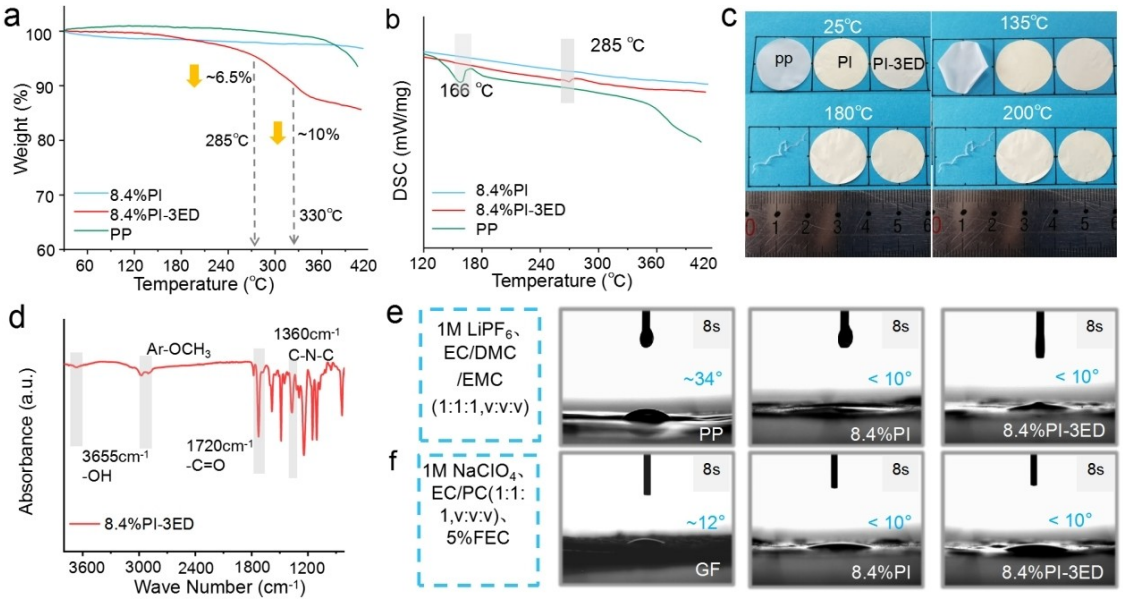

Figure 2. Thermal stability and wetting ability of PI and epoxy-strengthened separator, a) TG and b) DSC of PI, the strengthened and PP separator; c) photographs of samples at 25–200 °C; d) FT-IR of PI and PI-epoxy; e) contact angular of PP, GF, PI and the strengthened samples.

lower than 8.4% PI, 1.74 mS cm^{-1}, owing to the slightly lower porosity. Additionally, the conductivity of separators from 25 °C to 65 °C were detected in Figure S4 and then the activation energy were further calculated by plotting Arrhenius equation in Figure 3(b). 8.4% PI and 8.4% PI-3ED separator possess the close activation energy of ion transportation, 2.98 and 2.91 kJ mol^{-1}, obviously lower than that of PP, 7.55 kJ mol^{-1}.

Apart from promoting wettability, the abundant polar groups of PI could have effect on the transportation of Lithium ion. Thus, the Li^+ transference number was detected further and 0.81 is obtained for 8.4% PI separator and 0.72 for 8.4% PI-3ED in Figure 3(c). In comparison, only 0.36 is achieved for PP. More importantly, the anodic metal Lithium from the cycled $LiFePO_4$/Li cells containing 8.4%PI and 8.4%PI-3ED separators displayed the smoother and more even surface as reflected in Figure 3(d_1–d_3), implying the less lithium dendrite was evolved during the cycling. Presumably, the enhanced cycling stability could be accreted to the higher porosity and conductivity which reduce the diversified Li^+ concentration polarization on the surface of anode, compared the uneven pore distribution of PP separator in Figure S1. Simultaneously, Li symmetrical cells integrated with 8.4% PI and 8.4% PI-3ED were assembled to verify the promoted cycling stability of metallic lithium. Both cells show the stable and identical cyclability as long as 800 hrs in Figure 3(e). The abundant carbonyls and imines could provide extra more affinity than hydrocarbon groups. Therefore, the molecular dynamics simulation was conducted in Figure 3(f) which reveals the shorter distance, 1.39 Å and 1.42 Å, exists between Li^+ and the exposed polar groups than that between Li^+ and hydrocarbon, 2.15 Å. The shortened distance implies the stronger affinity, facilitating the shuttling of Li^+ by providing an extra pathway along the surface of PI and PI-3ED, as illustrated in Figure 3(g).

Subsequently, $LiFePO_4$/Li cells were assembled with 8.4% PI, 8.4% PI-3ED and PP respectively. In Figure 4(a), the PI, PI-3ED integrated cells display the superior rate capability to the PP-based cell. Figure 4(b) reveals the lower polarization of the 8.4% PI integrated cell due to the higher conductivity besides the outstanding cyclability of all cells, which are further confirmed in Figure 4(c and d) by comparing the charge and discharge profiles.

Along with the application in Lithium-based electrochemical system, the overcharge-sensitive PI separator was also attempted in Sodium-based electrochemical system. Likewise, the identical results have been achieved in Figures S5–S8, providing the possible employment in sodium-ion batteries.

Overcharge-sensitive PI-based separator

Besides insulating electrodes and conserving electrolyte, a functional separator was developed in recent years,[32] one of which can restrain overcharge by the conversion from the insulative state to the conductive state, precluding the irreversible electrochemical oxidation of the organic electrolyte. By virtue of the outstanding processability, overcharge-proof PI-based separator was developed by introducing coumarin-triphenylamine copolymer which possesses the excellent electrochemical activity and proper redox potential (3.7 V vs. Li), Figure S9. After optimization, 40 wt% proportion was adopted by compromising the effectiveness of overcharge-restraining and the strength of separator. The separator's microstructure is displayed in Figure 4(a), in which the sponge-like skeleton is still preserved integrally and the effectiveness was verified with $LiFePO_4$/Li half cell. In Figure 4(b), the voltage obviously ramps up at the end of full charge, and then enters a plateau at around 3.7 V owing to the short circuit from the conductive

Research Article
doi.org/10.1002/batt.202300244
Chemistry Europe
European Chemical Societies Publishing

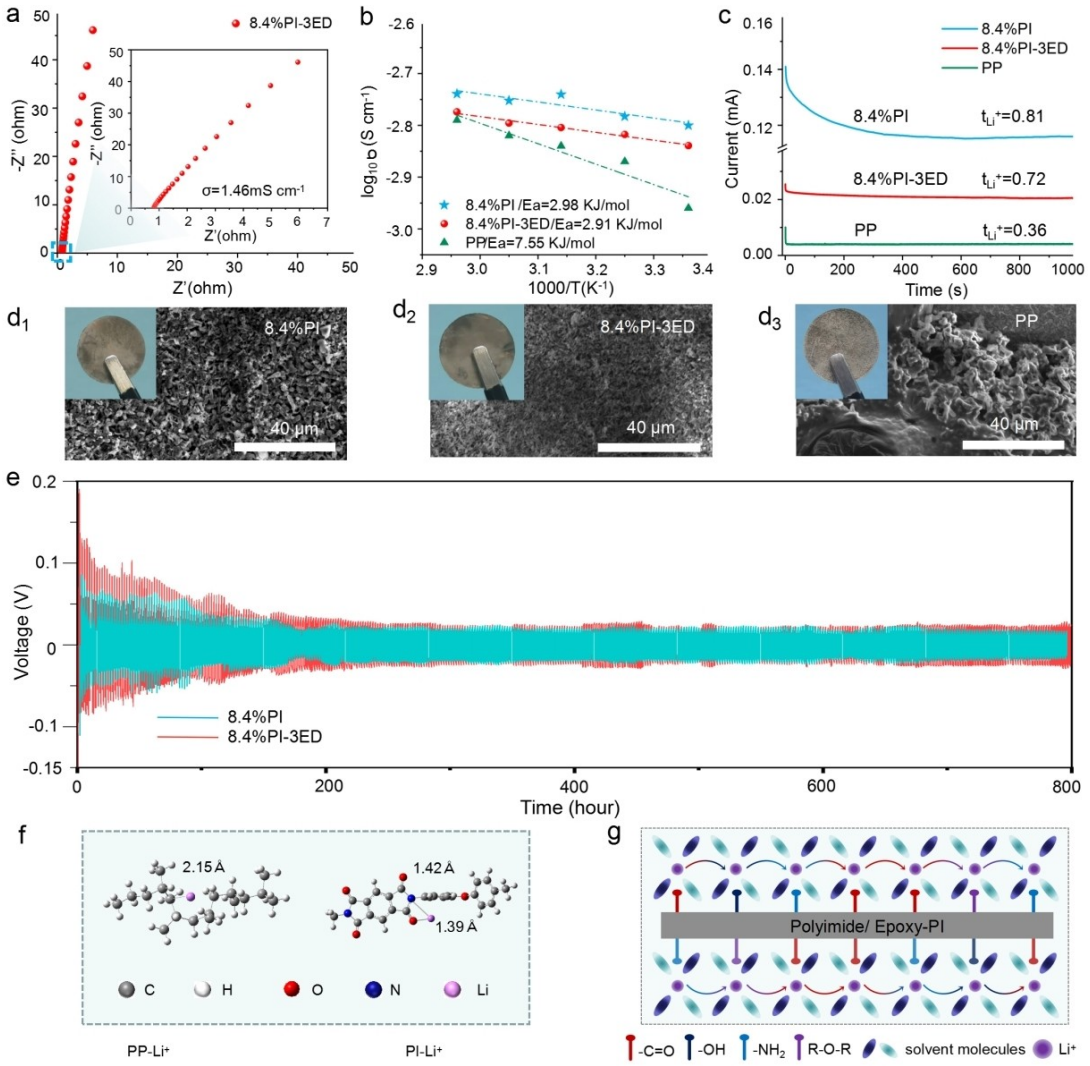

Figure 3. Performance of separators on ion transportation and in Li-based cell, a) EIS of 30 wt% epoxy-strengthened PI separator; b) activation energies obtained from linear fitting with Arrhenius equation; c) transference number of electrolyte-saturated PI, PI-3ED and PP separator; d_1–d_3) SEM of metal lithium anode; e) cycling performance of Li/Li symmetrical cell containing PI, epoxy-strengthened and PP separator; f) molecular dynamics simulation; g) schematic illustration of facilitated Li transportation.

transformation of the separator. The proper oxidation potential both ensures the cell is fully charged and avoids the oxidation of electrolyte. The coincident charge and discharge profiles imply the excellent electrochemical stability in the 1st, 11th and 21st cycle, too. Furthermore, the rate performance of over-charge-proof was investigated in Figure 5(c). In the beginning, the cell was charged at 0.6 mA cm^{-2} until overcharge to 3.7 V, and then the current density was promoted by 0.4 mA cm^{-2} every step. The restrained voltage is observed firstly, followed by the only tiny voltage lifting with the current promotion and then gradually fell down to 3.7 V, even at 3.4 mA cm^{-2}, displaying the excellent overcharge-proof rate performance. Subsequently, the cell releases all capacity during the normal discharge.

Conclusions

Targeted at the defects of polyolefin separator, the polyimide-based porous separator was facilely prepared by phase inversion. The resultant separator presents the favorable conductivity of 1.78 mS cm^{-1} and the higher transference number of 0.81, coming from its porosity of 87% and abundant polar groups, apart from the excellent thermal stability and wetting ability. By means of the strengthening tactic, the extra 30 wt% epoxy was introduced and the bearable stress was substantially promoted by 60%, from 3.1 MPa to 4.8 MPa, accompanying the only slight decrease in conductivity. Furthermore, by combining the conductive copolymer of coumarin-triphenylamine, the overcharge-sensitive separator was further developed and provided the stable and reliable protection for $LiFePO_4$-based lithium ion batteries even at 3.4 mA cm^{-2} during overcharge. Therefore, the preferable processability, the chemical and thermal stability and the wetting ability enable

Research Article
doi.org/10.1002/batt.202300244
Chemistry Europe
European Chemical Societies Publishing

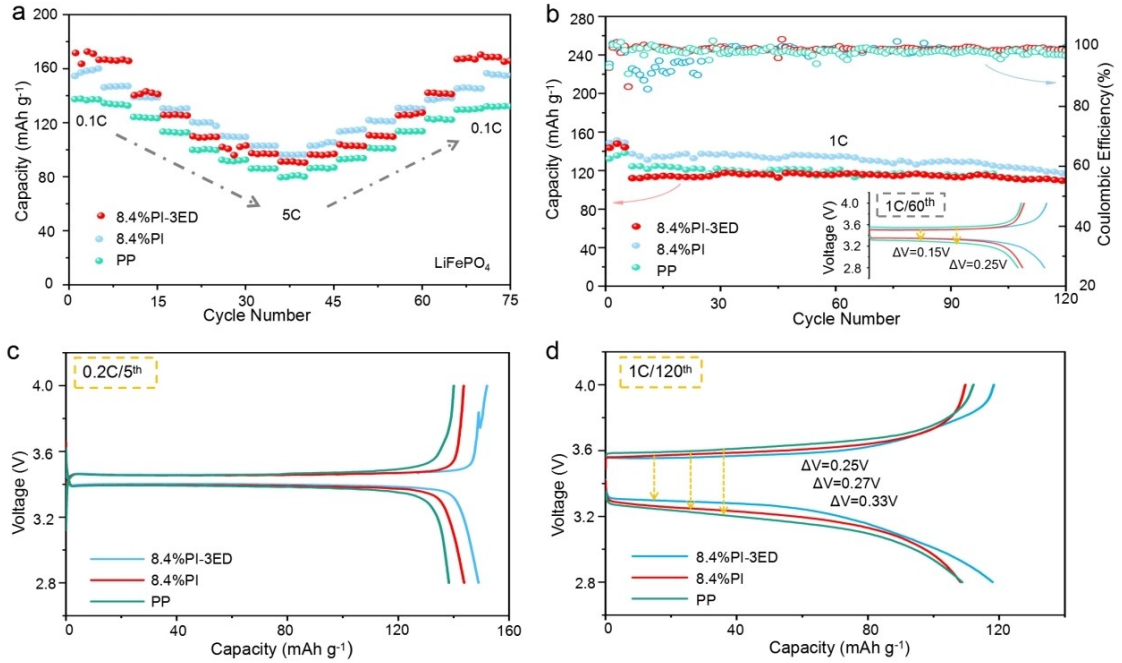

Figure 4. C-rate capability and cycling performance of the 8.4%PI-3ED, 8.4%PI and PP integrated cells in the range of 2.8–4.0 V, a) capacity from 0.1 C to 5 C; b) cyclability at 1 C; c and d) galvanostatic charge-discharge profiles of cells at 0.2 C and 1 C.

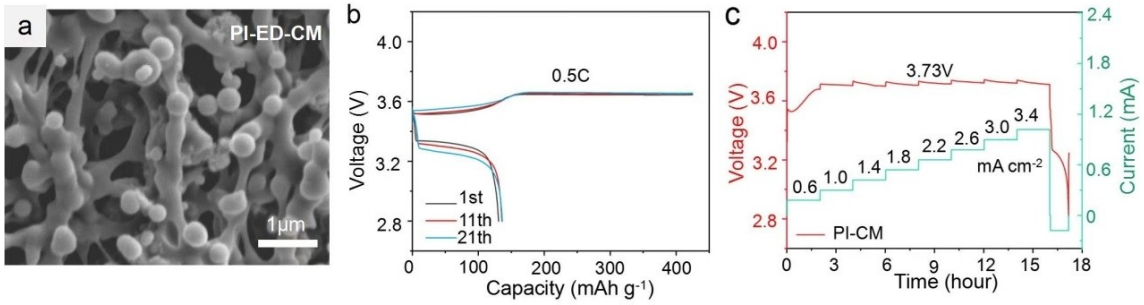

Figure 5. SEM, voltage-restraining behavior of overcharge-sensitive PI-based separator, a) SEM of PI separator containing conductive copolymer; b) voltage profile of $LiFePO_4$/Li during overcharge; c) voltage profile of overcharge-sensitive separator at the promoted current densities.

polyimide to be a greatly promising separator material for lithium/sodium-ion batteries.

Experimental Section

Preparation of porous polyimide and strengthened separator

Typically, 0.25 g polyimide powder (Macklin, molecular mass: 50–80 kDa) was thoroughly dissolved in 2.5 mL Dimethyl sulfoxide (DMSO, Sinopharm Chemical Reagent, Analytical Grade) to form 8.4 wt% solutions, then which was coated on the cleaned glass plate with a scraper. Simultaneously, the thickness of separators was controlled by adjusting the slit width of scraper. Afterwards, the solution-coated glass plate was transferred into deionized water and soaked for 36 hours to remove DMSO completely. Finally, the porous PI separator was obtained by slowly drying in air at room temperature. Likewise, a series of separators were prepared with the PI weight percentage of 6.8%, 8.4%, 10%, 12%, 14% and 16.7% by the identical steps, as well as an epoxy-strengthened separator by adding extra 10 wt%, 20 wt% and 30 wt% epoxy into 8.4 wt% PI-DMSO solution, labeled as 8.4%PI-ED, 8.4%PI-2ED and 8.4%PI-3ED, respectively. Glass fiber (Whatman, CAT NO. 1822-047) and polypropylene separator were also compared as blank samples.

Characterization of the separators

The morphology of separators was examined with Scanning Electronic Microscope (SEM, ZEISS Merlin Compact), and the mechanical property was evaluated by a stretching testing machine, STA449C. The polar groups of PI were verified by Fourier transform infrared spectroscopy (FTIR, Nicolet iS50). STA449F3 Synchronous Thermal Analyzer (NETZSCH Instruments Co., Ltd.) was employed to investigate the thermal stability from 25 °C to 400 °C with a heating rate of 10 °C min^{-1} under an argon atmosphere. The conductivity of electrolyte-saturated separators was detected with Electrochemical Impedance Spectroscopy (EIS, CHI 604e electrochemical workstation) in the range of 0.01 Hz–100 kHz.

Electrochemical measurement and cells assembly

Firstly, $LiFePO_4$ (LFP), super P and poly (vinylidene fluoride) (PVDF) in the weight percentage of 80/10/10 were uniformly dispersed in N-methylpyrrolidone (NMP) to form a black slurry, and then which was casted on Al foil. Thus, LFP cathodic sheet was obtained after drying at 60 °C overnight. Subsequently, 2025-type coin cells was assembled with anode of metallic Lithium and electrolyte (1 M $LiPF_6$, ethylene carbonate/dimethyl carbonate/ethyl methyl carbonate, 1 : 1 : 1 in volume, Dodochem, Suzhou, China)-saturated separator in argon-filled glovebox (Mikrouna, Super). The cells were evaluated by programmed Neware CT-4008 battery testing system (Shenzhen, China) at room temperature in voltage range of 2.8–4.0 V.

In addition, $Na_3V_2(PO_4)_3$ (NVP) and SnS_2-based coin cell was also assembled and assessed in the same procedure. Differently, the potential window was set between 2.5 and 4.0 V, and 1 M $NaClO_4$ EC/PC/5 wt% FEC was utilized.

Calculation of electrolyte uptake

The electrolyte uptake of the separators was calculated with the following Equation (1):

$$\text{Electrolyte uptake } (\%) = \frac{M - M_0}{M_0} \times 100\% \quad (1)$$

where M_0 and M are the weight of the pristine separator and the separator saturated in 1 M $LiPF_6$, EC/DMC/EMC (1 : 1 : 1, v/v/v) for 2 hours.

Calculation of ionic conductivity

The electrolyte-saturated separator was set between two stainless steel foil electrodes, and then measured by AC impedance, and the frequency ranges from 0.1 Hz to 10^5 kHz. The ionic conductivity rate can be calculated from Equation (2):

$$\sigma = \frac{L}{R_b \times S} \quad (2)$$

where L, R_b, and S are the thickness, the resistance and the area of separator, respectively.

Calculation of ionic transference number

According to the Bruce-Vincent method, DC polarization measurements were conducted with a potential of $\triangle V = 10$ mV for 1000 s in the Li |separator| Li cells until the current reached a steady state. Ionic transference number (t_{Li^+}) was calculated by the following Equation (3):

$$t_{Li^+} = \frac{I_S(\Delta V - I_0 R_0)}{I_0(\Delta V - I_S R_S)} \quad (3)$$

where I_s and I_0 account for the steady-state current and the initial current; ΔV is the voltage pulse by DC polarization; R_s and R_0 refer to the steady-state interfacial resistance and the initial interfacial resistance.

Activation energy (E_a)

The activation energy was calculated based on the plot of ionic conductivity (σ) vs. ($1/T$) from 25 °C to 65 °C according to Arrhenius equation (Equation (4)):

$$\sigma = Aexp\left(-\frac{E_a}{RT}\right) \quad (4)$$

Author Contributions

Xiangming Feng: Conceptualization, Methodology, Validation, Supervision, Mengzhen Wang: Investigation, Data curation, Writing- Original draft preparation. Jinyun Zheng: Resources. Junmin Ge: Reviewing and Editing, Mingrui Yang: Reviewing and Editing, Weihua Chen: Supervision, Project administration, Funding acquisition.

Acknowledgements

This work was supported by China Scholarship Council (CSC 202108410361), the National Natural Science Foundation of China (no. 22279121), Joint Fund of Scientific and Technological Research and Development Program of Henan Province (222301420009) and the funding of Zhengzhou University. Molecular dynamics simulation calculations were supported by the National Supercomputing Centre in Zhengzhou. The modification of manuscript was assisted by Prof. Qiong Cai, University of Surrey, UK.

Conflict of Interests

The authors declare that they do not have any conflict of interest with this manuscript.

Data Availability Statement

The authors declare that the data will be made available if needed.

Keywords: separator · polyimide · overcharge · conductive polymer · lithium-ion batteries

[1] B. Murdock, K. Toghill, N. Tapia-Ruiz, *Adv. Energy Mater.* **2021**, *11*, 2102028.
[2] C. Zhang, L. Shen, J. Shen, F. Liu, G. Chen, R. Tao, S. Ma, Y. Peng, Y. Lu, *Adv. Mater.* **2019**, *31*, 1808338.
[3] Y. Yang, E. Okonkwo, G. Huang, S. Xu, W. Sun, Y. He, *Energy Storage Mater.* **2021**, *36*, 186–212.
[4] Kai Liu, Yayuan Liu, Dingchang Lin, Allen Pei, Yi Cui, *Sci. Adv.* **2018**, *4*, eaas9820.
[5] P. Jaumaux, X. Yang, B. Zhang, J. Safaei, X. Tang, D. Zhou, C. Wang, G. Wang, *Angew. Chem. Int. Ed.* **2021**, *60*, 19965–19973.
[6] W. Seong, K. Park, M.. Lee, S. Moon, K. Oh, H. Park, S. Lee, K. Kang, *Energy Environ. Sci.* **2018**, *11*, 970–978.

[7] Q. Zhao, R. Wang, X. Hu, Y. Wang, G. Lu, Z. Yang, Q. Liu, X. Yang, F. Pan, C. Xu, *Adv. Sci.* **2022**, *9*, 2102215.
[8] X. Li, J. Zhang, X. Guo, C. Peng, K. Song, W. Chen, *Adv. Mater.* **2023**, 2203547.
[9] Y. Wan, K. Song, W. Chen, X. Zhang, J. Zhang, *Angew. Chem. Int. Ed.* **2021**, *60*, 11481–11486.
[10] K. Song, X. Wang, Z. Xie, J. Luo, W. Chen, *Angew. Chem. Int. Ed.* **2023**, e202216450.
[11] W. Li, C. Liu, W. Chen, C. Shen, *Adv. Energy Mater.* **2023**, 2300648.
[12] C. Ma, X. Wang, J. Lan, J. Zhang, K. Song, J. Chen, J. Ge, W. Chen, *Adv. Funct. Mater.* **2022**, 2211821.
[13] Y. Mao, W. Sun, Y. Qiao, X. Liu, C. Xu, L.i. Fang, W. Hou, Z. Wang, K. Sun, *Chem. Eng. J.* **2021**, *416*, 129119.
[14] W. Chen, L. Zhang, C. Liu, X. Feng, J Zhang, L. Guan, L. Mi, S Cui, *ACS Appl. Mater. Interfaces* **2018**, *10(28)*, 23883–23890.
[15] X. Guo, X. Li, Y. Xu, J. Chen, M. Lv, M. Yang, W. Chen, *J. Phys. Chem. C.* **2022**, *126*, 8238–8247.
[16] J. Zheng, J. Zhang, W. Li, J. Ge, W. Chen, *Chem. Eng. J.* **2023**, *465*, 142796.
[17] G. Feng, Z. Li, L. Mi, J. Zheng, X. Feng, W. Chen, *J. Power Sources* **2018**, *376*, 177.
[18] H. Zhang, L. Sheng, Y. Bai, S. Song, G. Liu, H. Xue, T. Wang, X. Huang, J. He, *Adv. Eng. Mater.* **2020**, *22*, 1901545.
[19] Y. Deng, Y. Pan, Z. Zhang, Y. Fu, L. Gong, H. Zhang, X. Cheng, *Adv. Funct. Mater.* **2022**, *32*, 2106176.
[20] J. Deng, D. Cao, X. Yang, G. Zhang, *Chem. Eng. J.* **2022**, *433*, 133934.
[21] Chen Y, Luo J, Xu H, X. Hou, M. Gong, C. Yang, H. Liu, X. Wei, L. Zhou, C. Yin, X. Li, *ACS Appl. Energ. Mater.* **2023**, *6*, 1692–1701.
[22] Z. Lu, F. Sui, Y. Miao, G. Liu, C. Li, W. Dong, J. Cui, T. Liu, J. Wu, C. Yang, *J. Energy Chem.* **2021**, *58*, 170–197.
[23] G. Sun, L. Kong, B. Liu, H. Niu, M. Zhang, G. Tian, S. Qi, D. Wu, *J. Membr. Sci.* **2019**, *582*, 132–139.
[24] N. Bratasyuk, V. Zuev, *Thermochim. Acta* **2020**, *687*, 178598.
[25] L. He, L. Liu, C. Cao, F. Jiang, J. Xu, *J. Adhes. Sci. Technol.* **2021**, 1929003.
[26] D. Lu, S. Lin, S. Hu, W. Cui, T. Fang, A. Iqbal, Z. Zhang, W. Peng, *J. Solid State Electrochem.* **2021**, *25*, 315–325.
[27] P. Chombo, Y. Laoonual, *J. Power Sources* **2020**, *478*, 228649.
[28] X. Feng, J. Zheng, J. Zhang, R. Li, Z. Li, *Electrochim. Acta* **2009**, *54*, 4036–4039.
[29] E. Beletskii, A. Fedorova, D. Lukyanov, A. Kalnin, V. Ershov, S. Danilov, D. Spiridonova, E. Alekseeva, O. Levin, *J. Power Sources* **2021**, *490*, 229548.
[30] L. Zhang, G. Feng, X. Li, S. Cui, S. Ying, X. Feng, L. Mi, W. Chen, *J. Membr. Sci.* **2019**, *577*, 137–144.
[31] L. Yu, L. Yu, Y. Peng, X. Lan, X. Hu, *Mater. Today Phys.* **2022**, *25*, 100716.
[32] S. Tajik, H. Beitollahi, F. Nejad, I. Shoaie, M. Khalilzadeh, M. Asl, Q. Le, K. Zhang, H. Jang, M. Shokouhimehr, *RSC Adv.* **2020**, *10*, 37834–37856.

Manuscript received: June 10, 2023
Revised manuscript received: July 25, 2023
Accepted manuscript online: July 31, 2023
Version of record online: October 20, 2023